Journal of Power Sources 222 (2013) 351–358

Contents lists available at SciVerse ScienceDirect

Journal of Power Sources

journal homepage: www.elsevier.com/locate/jpowsour

Short communication

C/CrN multilayer coating for polymer electrolyte membrane fuel cell metallic bipolar plates

Kai Feng [a], Zhuguo Li [a,*], Hailin Sun [b], Lei Yu [c], Xun Cai [a], Yixiong Wu [a], Paul K. Chu [d]

[a] Shanghai Key laboratory of Materials Laser Processing and Modification, School of Materials Science and Engineering, Shanghai Jiao Tong University, Shanghai 200240, China
[b] Teer Coatings Ltd, Miba Coating Group, UK
[c] Zhejiang Huijin-Teer Coatings Co., Ltd., Lin'an 311305, China
[d] Department of Physics and Materials Science, City University of Hong Kong, Tat Chee Avenue, Kowloon, Hong Kong, China

HIGHLIGHTS

► C/CrN multilayer coatings with dense structure and high percentage of sp^2 bond are deposited on SS316L.
► C/CrN multilayer coatings exhibit superior surface conductivity that is even better than that of graphite.
► Electrochemical results disclose that the C/CrN multilayer coatings have excellent corrosion resistance.

ARTICLE INFO

Article history:
Received 6 July 2012
Received in revised form
29 August 2012
Accepted 30 August 2012
Available online 7 September 2012

Keywords:
Multilayer
Bipolar plates
Magnetron sputtering
Interfacial contact resistance
Corrosion resistance
Fuel cell

ABSTRACT

The two most important issues that plague wider use of stainless steel bipolar plates in polymer electrolyte membrane fuel cells (PEMFCs) are insufficient corrosion resistance and surface conductivity. In this study, C/CrN multilayer coatings are deposited on 316L stainless steel samples by close-field unbalanced magnetron sputtering ion plating. SEM shows that the C/CrN coatings are dense, continuous, and composing of carbon granules on the surface. Raman spectroscopy reveals an amorphous structure with a large sp^2 constituent. The corrosion resistance and interfacial contact resistance (ICR) are investigated systematically. A superior ICR in the range of 2.6–2.9 mΩ-cm^2 at a compaction force of 150 N/cm^2 is achieved and it is even better than that of graphite. The deposited film possesses high chemical inertness thereby significantly enhancing the corrosion resistance of the coated SS316L. A thickness of 800 nm is sufficient to protect against corrosion. C/CrN multilayer coatings are beneficial in that it can lead to a faster PVD deposition process and lower material cost, while permitting a superior performance in terms of surface conductivity and corrosion resistance.

1. Introduction

Polymer electrolyte membrane fuel cells (PEMFCs) have attracted much research and practical interests due to growing environmental concerns and limited fossil fuel reserves. It is in fact one of the most promising power sources for transportation and distributed power generation because of the high efficiency and power density, carbon emission-free operation, and low working temperature [1]. However, the high manufacturing cost and insufficient durability have prevented PEMFCs from wider commercial acceptance.

The bipolar plates (BBPs) are a key multifunctional component in the PEMFCs contributing over 80% of the total stack weight, more than 20% of materials cost, and 10% total fuel cell stack cost [2]. They serve to separate individual cells, act as both the anode and cathode, collect the electrical current from the fuel cells, introduce the reactive gases, and remove the heat and exhaust water [3]. Technically, BBPs must have high interfacial electrical conductivity, good corrosion resistance, high gas impermeability, good mechanical performance and low cost [4]. Stainless steels are one of the suitable bipolar plate materials because they can satisfy most requirements [4–7]. However, surface modifications are still required in order to enhance the interfacial electrical conductivity, inhibit corrosion, and ensure adequate service life in the harsh PEMFC working environment [8–10]. A thinner surface coating, which enhances the power density and offers easier thermal management and reduced packaging requirements, is especially attractive in commercial applications. The service lifetime can also be addressed by improving the recyclability of coated stainless steel BBPs.

* Corresponding author. Tel.: +86 21 34202837; fax: +86 21 34203024.
E-mail address: lizg@sjtu.edu.cn (Z. Li).

0378-7753/$ – see front matter
http://dx.doi.org/10.1016/j.jpowsour.2012.08.087

Many types of coatings prepared by various methods have been investigated as possible bipolar plate materials. For example, metal nitrides coatings such as TiN and CrN prepared by physical vapor deposition (PVD) have received increasing attention due to the electrical conductivity [11] and high chemical inertness [12–19]. However, these metal nitride coatings are prone to local corrosion and the corrosion current density has been reported to increase dramatically after long time immersion in the simulated PEMFC environment [16,17]. This mainly arises from defects in the coating such as pinholes and macroparticles created during PVD [20]. In order to eliminate pinholes in the coatings, multilayer coatings have been deposited on metallic bipolar plates. Zhang et al. [21,22] deposited Cr/CrN/Cr multilayers on stainless steel 316L (SS316L) by arc ion plating. It was observed that the corrosion current density in the simulated anode and cathode environments diminished by one order of magnitude and the interfacial contact resistance (ICR) at 150 N cm^{-2} dropped to 30–35 mΩ-cm^2 [21]. Tian [23] produced CrN/Cr multilayers on SS316L to increase the corrosion resistance and surface conductivity, and a current density approaching to 1 $\mu A/cm^2$ and ICR of 35 mΩ-cm^2 at a compaction force of 150 N/cm^2 were achieved.

Compared to metal nitrides coatings, amorphous carbon coatings possess higher electrical conductivity and chemical inertness. We have successfully deposited dense and adherent amorphous carbon coating on SS316L by closed field unbalanced magnetron sputtering ion plating (CFUBMSIP) [24–26]. This coating has good corrosion resistance and also excellent surface conductivity that is even better than that of graphite due to the relatively large sp^2 component. Nevertheless, the deposition rate is quite small and it usually takes several hours to deposit a thick enough coating due to the extremely low sputtering yield of carbon (usually lower than 0.1) during the PVD process. In this paper, we describe a new multilayer coating composed of amorphous carbon as the outer layer and CrN as the inner layer (C/CrN multilayer). Combining both of these coatings together could be an effective way, in terms of both process efficiency and economics, to produce low-cost coatings for the performance enhancement and protection of stainless steel BPPs in PEMFC.

2. Experimental details

2.1. Substrate materials

The substrate in this study was SS316L purchased from Trinity Brand Industries (TBI) Inc., US with the following chemical compositions: C < 0.03%, Si < 1%, Mn < 2%, Ni 8–12%, Cr 16–18%, Mo 2–3%, S < 0.03%, P < 0.04%, and Fe balance. The SS316L samples were cut into 12 mm × 12 mm × 4 mm pieces, polished with No. 1500 SiC waterproof abrasive paper, cleaned with acetone and distilled water in an ultrasonic bath, and dried before subjecting to PVD.

2.2. Coating design and deposition parameters

All the coatings were deposited on a Teer UDP 650 CFUBMSIP system. Deposition was carried out using a high density of low energy bombarding ions, thus resulting in very dense, non-columnar coating structures with low internal stress. The C/CrN multilayer coatings were deposited using two chromium targets and two graphite (C) targets. After the chamber was pumped down to a pressure of 2.0–3.5 × 10^{-5} torr, argon was introduced to reach a working pressure between 8.0×10^{-4} and 2.0×10^{-3} torr depending on the required coating. The detail deposition parameters are shown in Table 1. Prior to deposition, the substrate was biased to −500 V and a small current of 0.4 A was applied to each Cr magnetron target to clean and remove the native passive film on the surface. A thin (~100 nm) Cr metallic seed layer was deposited when 6 A was supplied to each Cr target to enhance adhesion. Afterward, a CrN layer was reactively sputtered in a mixture of argon and nitrogen and the flow rates were controlled to yield the required coating stoichiometry. Before deposition of the carbon coating, a thin intermediate CrN layer doped with carbon was deposited as an interfacial layer by reducing the current supplied to the Cr target(s) and increasing simultaneously the current supplied to the carbon targets from 0.2 A to 7 A. Finally, the carbon layers were deposited. The carbon coatings deposited for 1800, 3600, 5400, and 7200 s are designated as C/CrN-1, C/CrN-2, C/CrN-3, and C/CrN-4, respectively in this work.

2.3. Characterization

The surface morphology and cross section of the C/CrN multilayer coatings were examined by field-emission scanning electron microscopy (FE-SEM) of HITACHI S-4800. Energy-dispersive X-ray spectroscopy (EDS) was carried out to determine the cross-section chemical distribution. The surface morphology after potentiostatic tests was observed in order to investigate the mechanism and extent of corrosion on the surface. Raman spectroscopy was conducted on the Bruker Optics Senterra R200-L to determine the chemical structure.

2.4. ICR measurement

The ICR was measured from the structures consisting of two pieces of conductive carbon paper (Toray TGP-H-090) sandwiched between the sample and two copper plates. A constant current of 0.1 A was applied through the two copper plates and the voltage was monitored as a function of steadily increasing compaction force. More details about the procedures can be found in the literature [9].

2.5. Electrochemical tests and ICP measurement

Potentiodynamic tests, potentiostatic tests, and inductively coupled plasma atomic emission spectrometry (ICP-AES) were conducted on the Zahner Zennium electrochemical workstation to evaluate the corrosion resistance and corrosion rate of the bare and C/CrN multilayer-coated SS316L. The three-electrode system comprising a platinum sheet (counter electrode), saturated calomel electrode (SCE, as the reference electrode), and sample (working electrode) was used. The electrochemical tests were conducted in 0.5 M H_2SO_4 + 2 ppm HF solution at 80 °C to simulate the

Table 1
Detailed deposition parameters.

Deposition process	Cr target current (A)	C target current (A)	Bias voltage (V)	N_2 gas flow rate (SCCM)	Ar gas flow rate (SCCM)	Deposition time (s)
Cleansing	0.4	–	−500	–	30	600
Cr transition layer	6	–	−60	–	30	300
CrN coating	6	–	−60	25	30	1100
C coating	–	7	−60	–	15	1800, 3600, 5400, 7200

aggressive PEMFC environment. The solution was purged with either air (to simulate cathode environment) or hydrogen gas (to simulate anode environment) prior to and during the electrochemical test. Before the electrochemical test, the open circuit potential (OCP) versus time was recorded for 1 h to ensure electrochemical stability. Potentiodynamic polarization was performed at a potential scanning rate of 1 mV s^{-1}. The potentiostatic test was carried out to investigate the performance and stability of the bare and C/CrN multilayer-coated samples in the aggressive PEMFC environment. It was conducted for 10 h at a potential of 0.6 V versus SCE while purging with air and −0.1 V vs SCE while purging with H_2 to simulate the cathode and anode operating environments, respectively. The experimental error of the current in the electrochemical test was within 0.05% in the range of 1 nA to 2.5 A. After the potentiostatic test, the solution (∼100 mL) was collected and analyzed by inductively coupled plasma atomic emission spectrometry (ICP-AES) to determine the amounts of Fe, Cr, and Ni ions released to the solutions. ICP-AES showed a relative standard deviation of 1% due to the variability in the plasma, pumping rate, and nebulizer efficiency.

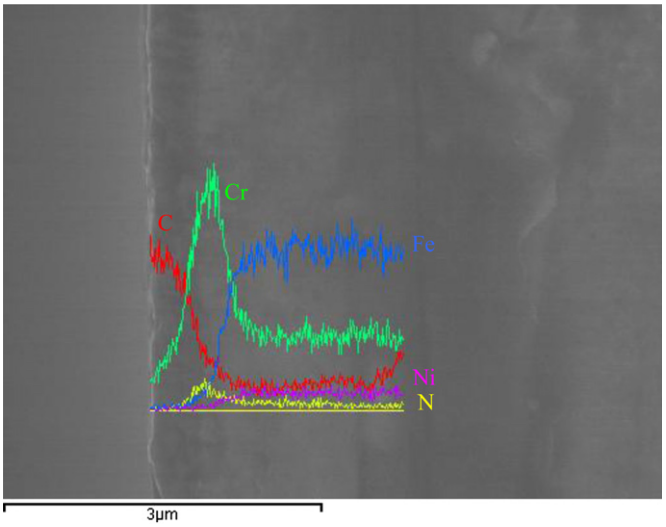

Fig. 2. SEM cross-section and EDS line-scan of the C/CrN-3 samples.

3. Results and discussion

3.1. Surface morphology

The surface morphology and cross-section of the C/CrN multilayer coatings on SS316L observed by SEM are shown in Figs. 1 and 2, respectively. The C/CrN multilayer coatings, which show carbon granules with diameters ranging from 100 to 400 nm are compact and dense covering the entire stainless steel substrate. In the deposition process, the coating near the substrate consists of randomly arranged small particles out of which V-shaped columns emerge slowly and overgrow the kinetically unfavored columns. In general, a larger particle size in two dimensions in the SEM results indicates larger density of the coating. The diameter of the carbon granules increases with deposition time and so the coating deposited for a longer time has a denser structure. The cross-sectional SEM and EDS line-scans of C, Cr, N, Fe, and Ni of C/CrN-3 sample are

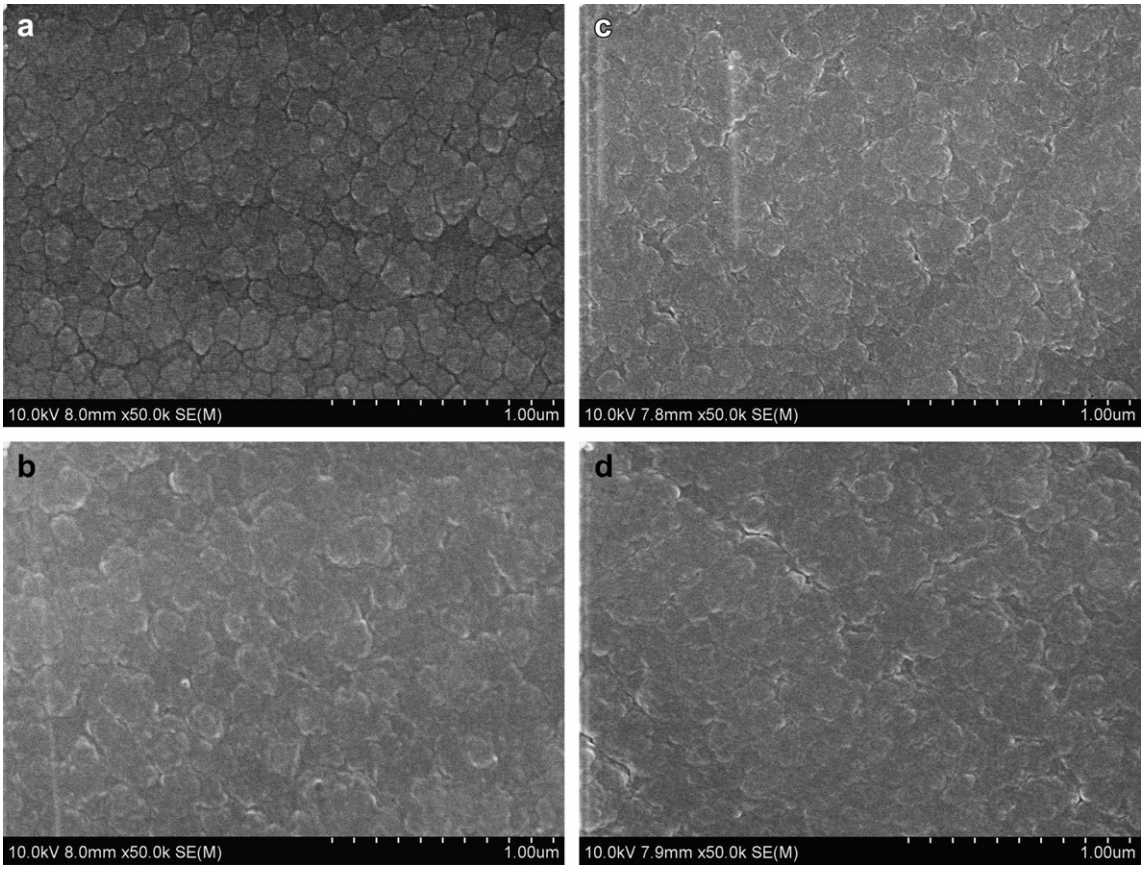

Fig. 1. SEM images of the surface morphology of the C/CrN multilayer coating on SS316L: (a) C/CrN-1, (b) C/CrN-2, (c) C/CrN-3, (d) C/CrN-4.

shown in Fig. 2. The C/CrN multilayer coatings are uniform and dense and bond well to the SS316L substrate. Consequently, the C/CrN multilayer coating is expected to prevent the substrate from direct corrosion. The total coating thickness is about 800 nm whereas the carbon coating is approximately 400 nm thick. Assuming the deposition rate is constant within the deposition time, the carbon coating thicknesses of C/CrN-1, C/CrN-2 and C/CrN-4 samples are estimated to be about 130 nm, 260 nm and 530 nm, respectively.

3.2. Raman analysis

Fig. 3 depicts the Raman spectrum of the C/CrN-4 sample. The Raman spectrum of C/CrN-4 is typical of a graphite-like carbon film [27]. It consists of a large amount of sp^2 in the two-dimensional graphite lattice or three-dimensional graphite microcrystals within a diameter of 30 nm and disorder bonds at the boundaries of the graphite microcrystals. To reveal more information about the structure, the Raman spectrum is deconvoluted by two Gaussian peaks. The D-bond around 1360 cm^{-1} corresponds to the disordered bond originating from disordered structure in the graphite lattice [27] and the peak at approximately 1560 cm^{-1} is due to bond stretching of pairs of sp^2 atoms in both rings and chains. The integrated area of the D-bond is higher than that of the G-bond, indicating that the proportion of disordered structure is larger. However, both the G and D bonds are due to sp^2 bond only. The G peak is due to the bond stretching of pairs of sp^2 atoms in both rings and chains, whereas the D peak is due to the breathing modes of the A1g symmetry involving phonons near the K zone boundary. This mode is forbidden in perfect graphite and only becomes active in the presence of disorder [28,29].

3.3. Interfacial contact resistance (ICR)

The ICR values of C/CrN multilayer-coated SS316L samples are investigated as a function of compaction force (shown as Fig. 4) with graphite as the reference. In general, the ICR decreases with compaction force logarithmically, indicating that the compaction force is dominant in the reduction of the ICR in the region with lower compaction force while the surface composition is the predominant factor in the region with higher compact force. The bare SS316L exhibits a higher ICR value of 370.1 mΩ-cm^2 at 150 N cm^{-2} because the thin oxide layer produces a surface passivation state [30]. However, the ICR of the C/CrN multilayer-coated SS316L is much

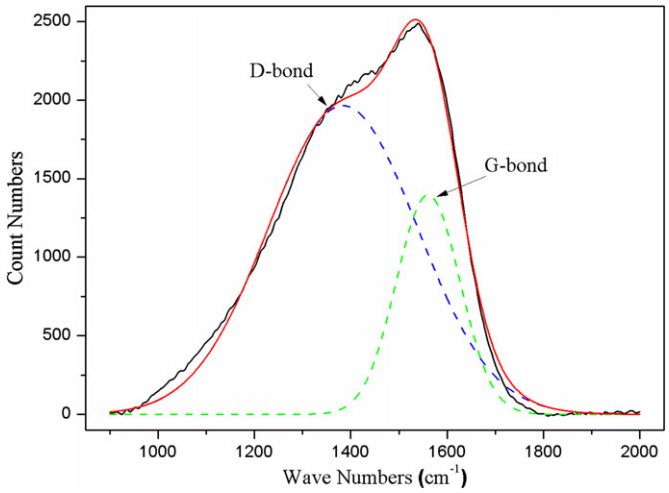

Fig. 3. Raman spectrum of the C/CrN multilayer coating on SS316L.

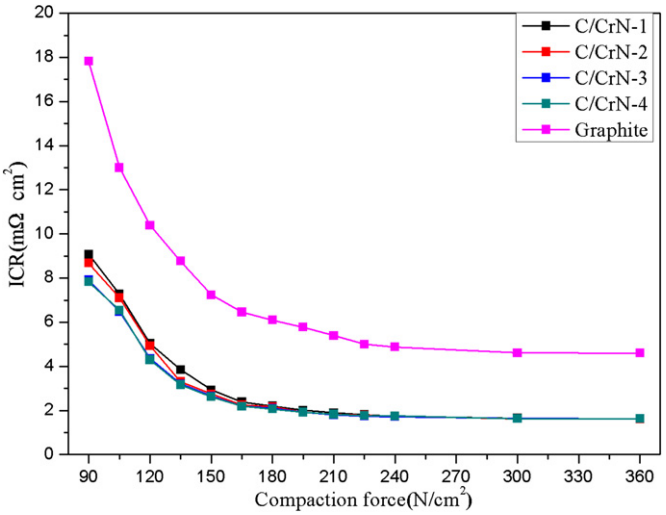

Fig. 4. Variation of the ICR values versus compaction force determined from the C/CrN multilayer-coated SS316L samples as well as graphite.

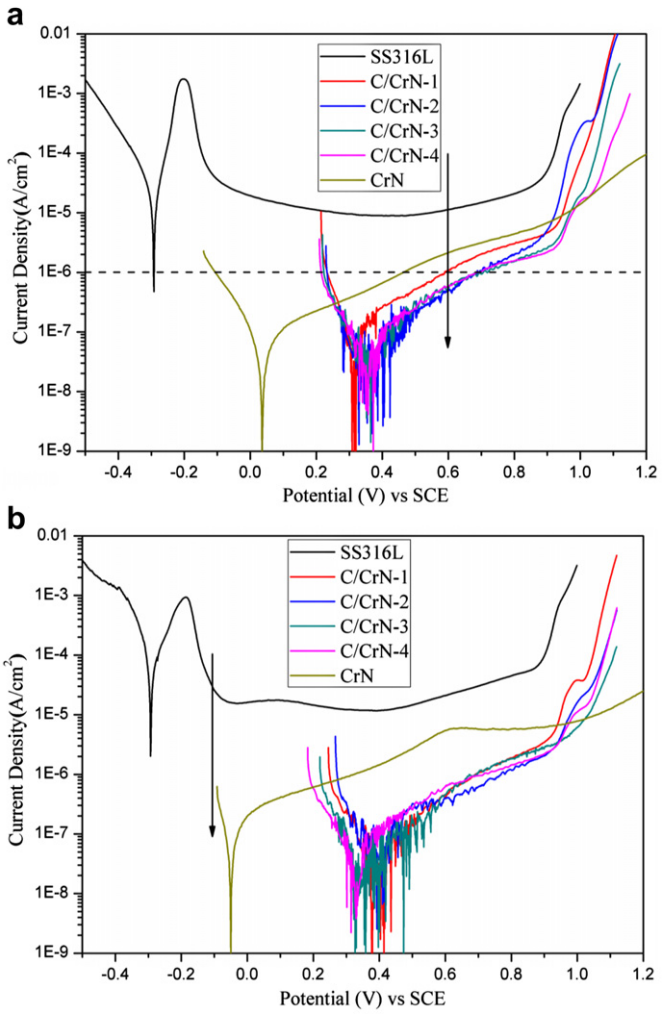

Fig. 5. Potentiodynamic curves obtained from the bare and C/CrN multilayer-coated SS316L in the simulated aggressive PEMFC solution: (a) purged with air and (b) purged with H_2.

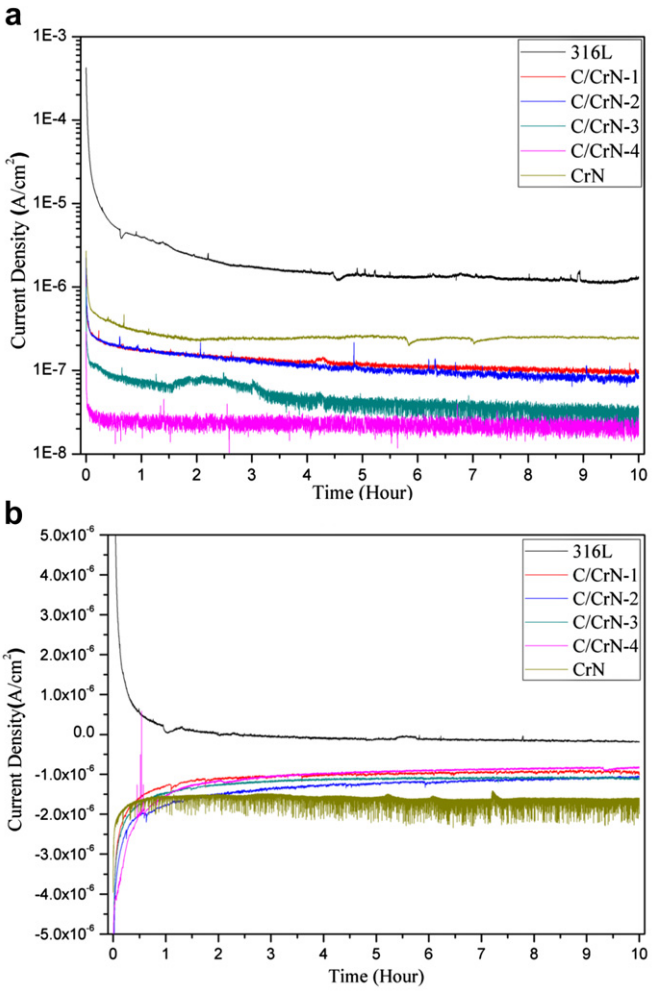

Fig. 6. Potentiostatic curves of the bare and C/CrN multilayer-coated SS316L in the (a) simulated cathode (0.6 V vs SCE purged with air) and (b) anode environment (−0.1 V vs SCE purged with H_2).

smaller, in the range 2.6–2.9 mΩ-cm^2 at 150 N-cm^{-2}, even when the carbon coating thicknesses are varied. The ICR of the C/CrN-coated stainless steel decreases slightly with increasing carbon coating thickness. It is known that the ICR is mainly influenced by the conductivity of the sample surface, which is further affected by the nature of the coating materials such as the chemical composition, density, and bonding type. In this case, as the chemical composition and bonding type are same, the slight reduction in the ICR with coating thickness can be attributed to the increase in the density of the thicker coating. Fig. 4 shows that the ICR of the C/CrN multilayer-coated SS316L is even lower than that of graphite and it is slightly smaller for the thicker carbon coating due to the good electrical conductivity. In particular, the coatings show superior conductivity compared to TiN and CrN, about 30 mΩ-cm^2 [31] and 10 mΩ-cm^2 [14,15] at typical compaction forces, respectively, and it even approaches that of a 10 nm thick Au film on stainless steel [5]. Compared to the ICR of the amorphous carbon coating previous reported (6.8 mΩ-cm^2 at compaction force of 150 N cm^{-2}) [24,25], the C/CrN multilayer has an even better surface conductivity. The ICR is influenced by both the contact area between the sample and carbon paper as well as conductivity of the sample surface, which is further affected by the composition of the coating materials. Therefore, as the contact area exerting the same compaction force is identical, the overall reduction in ICR by the C/CrN multilayer coating can be attributed to the incorporation of CrN coating. The ICR results thus clearly indicate that the C/CrN multilayer coatings can significantly improve the surface conductivity of the stainless steel BPPs.

3.4. Potentiodynamic test

The corrosion resistance is one of the most important characteristics of BPP materials in fuel cells. The potentiodynamic polarization behavior of the bare and C/CrN multilayer-coated SS316L in 0.5 M H_2SO_4 + 2 ppm HF is shown in Fig. 5. SS316L shows a negative corrosion potential around −0.3 V in both the cathode and anode environments, while the corrosion potential of C/CrN multilayer-coated SS316L shifts to the positive direction ranging from 0.3 V to 0.4 V. Thermodynamically, a higher corrosion potential means higher chemical inertness and better corrosion resistance. In the cathode environment, SS316L exhibits a broader passive region ranging from −0.1 V to 0.9 V, in which the passivation current density maintains its value regardless of potential increase. However, the passivation current density at the cathodic operation potential (0.6 V) is as high as 11.26 μA-cm^{-2} which is still unacceptable for applications of bipolar plate materials. CrN-coated SS316L shows a corrosion potential of about 0.04 V and a passivation current density at 0.6 V of 2.14 μA-cm^{-2}. As for the C/CrN multilayer-coated SS316L, although they exhibit a different polarization behavior and narrower passive region, the passivation current density at 0.6 V is significantly reduced to 0.50–1.06 μA-cm^{-2}. It is noted that C/CrN-1 displays a higher passivation current density and C/CrN-2 shows an unstable current density in the range of 0.4–0.6 V caused by the breakdown and re-passivation of the surface coating as the external applied voltage is scanned. This result indicates that the carbon coating with such a thickness probably cannot provide sufficient protection. In the anode environment, the anode potential is at the margin of the active region of the SS316L resulting in unstable passivation under this condition. For CrN-coated SS316L sample, the corrosion potential is about −0.05 V, which is nobler than anode operation potential of −0.1 V. The corrosion potential of the C/CrN multilayer-coated SS316L shifts toward the positive direction reaches about 0.2–0.3 V which is much nobler than the anodic operation potential (−0.1 V). Hence, the coatings provide good protection for the stainless steel BPPs under the anodic environmental conditions. The potentiodynamic test results indicate that coatings provide higher chemical inertness and better corrosion resistance in both the cathode and anode environments.

Table 2
Fe, Cr, Ni ion concentrations released from the bare and C/CrN multilayer-coated SS316L samples after potentiostatic test.

Sample	Ion concentration in PEMFC cathode environment after 10 h (ppm)				Ion concentration in PEMFC anode environment after 10 h (ppm)			
	Fe	Cr	Ni	Total	Fe	Cr	Ni	Total
SS316L	7.62	0.88	0.69	9.19	6.28	0.90	0.61	7.79
C/CrN-1	1.209	0.021	0.039	1.269	1.753	0.011	–	1.764
C/CrN-2	1.278	0.032	0.019	1.329	0.281	0.007	–	0.288
C/CrN-3	0.614	0.025	0.025	0.664	0.651	0.015	–	0.666
C/CrN-4	0.191	0.002	–	0.193	0.231	0.005	–	0.236

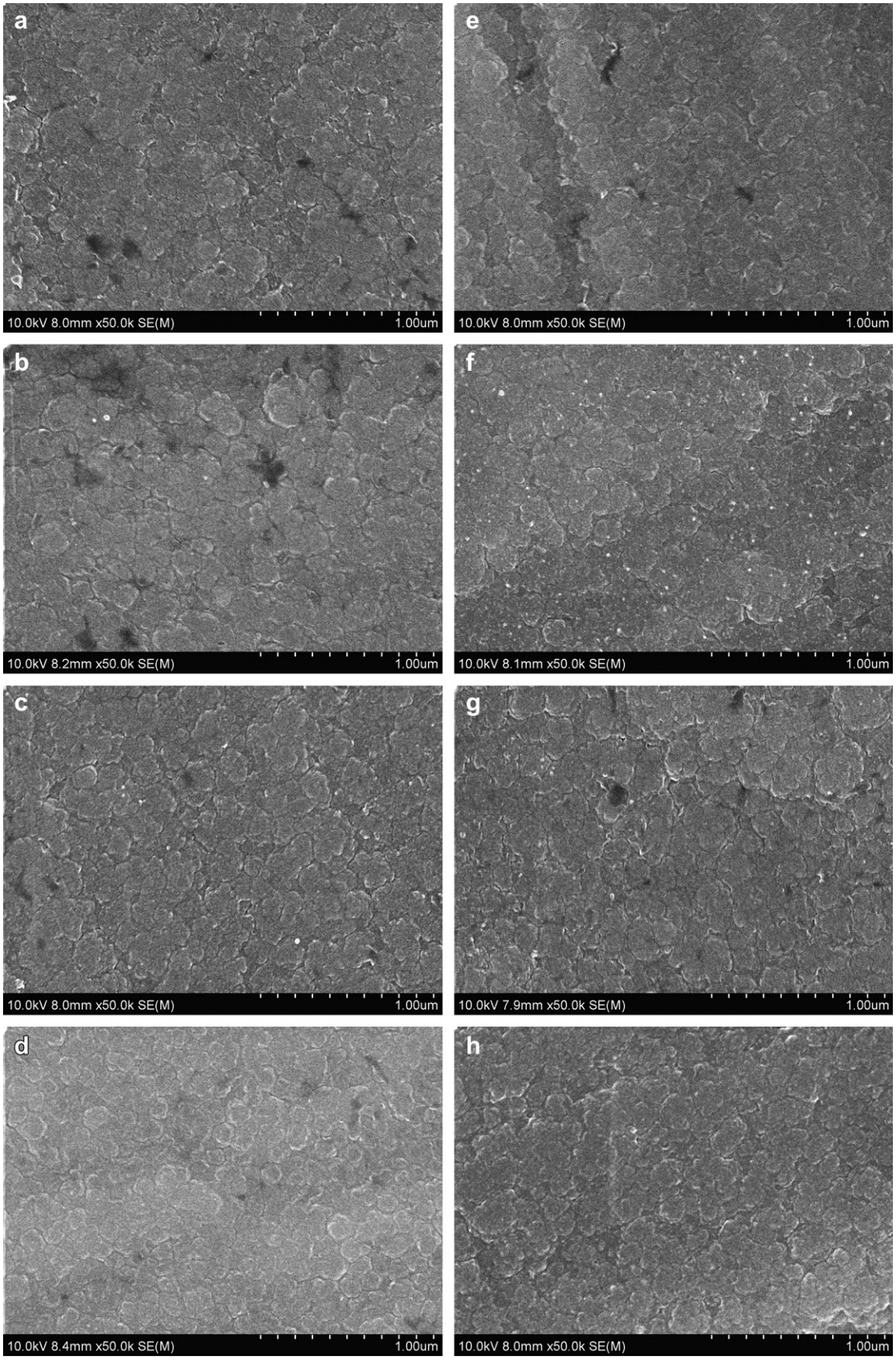

Fig. 7. Surface morphology after potentiostatic test in the cathode environment: (a) C/CrN-1, (b) C/CrN-2, (c) C/CrN-3, (d) C/CrN-4; and in the anode environment: (e) C/CrN-1, (f) C/CrN-2, (g) C/CrN-3, (h) C/CrN-4.

3.5. Potentiostatic test and ICP measurement

The bipolar plate under the real PEMFC working conditions is subjected to corrosion at an applied potential (cathode 0.6 V vs SCE; anode −0.1 V vs SCE) which is different from the free corrosion potential. Therefore, the potentiostatic test is conducted to benchmark the corrosion resistance in the aggressive PEMFC environment. In the cathode environment, 0.6 V vs SCE is applied during the potentiostatic test while purging with air whereas in the anode environment, −0.1 V vs SCE is applied while purging with H_2. Fig. 6(a) shows that the current density of the bare SS316L decreases rapidly in the beginning and then stabilizes at around 1.3 μA-cm^{-2} in the cathode environment. The fast drop in the current density is due to the reformation of the passive film. As soon as the whole surface is covered by a new passive film, the current density needed to maintain passivation is relatively low. CrN-coated SS316L sample exhibits a current density of around 0.25 μA-cm^{-2}, which is lower than that of the bare SS316L while higher than that of C/CrN multilayer-coated SS316L. With regard to the C/CrN multilayer-coated SS316L, the current densities are maintained at much lower values compared to SS316L of around 90 pA-cm^{-2} for C/CrN-1 and C/CrN-2 and 20 pA-cm^{-2} for C/CrN-3 and C/CrN-4. In general, a lower current density means less electrochemical reaction on the interface between the solid surface and adjacent electrolyte as well as smaller metal ion release rates. Therefore, it is expected the amounts of released metal ions from the SS316L can be significantly reduced by this C/CrN multilayer coating. Compared to the C/CrN multilayer coating with different carbon coating thicknesses, the current densities of C/CrN-1 and C/CrN-2 are higher than those of C/CrN-3 and C/CrN-4 due to the insufficient carbon coating thickness. Fig. 6(b) displays the potentiostatic curves at −0.1 V vs SCE in the anode environment. The current density of SS316L decays dramatically, undergoes a positive–negative switch, and then gradually heads to the positive direction finally stabilizing at a relatively low negative level. The current density of CrN-coated SS316L undergoes vibration at a relative negative level, indicating that the CrN coating is unstable in the anode environment. The current measured from the C/CrN multilayer-coated SS316L exhibits a different polarization behavior. It increases in the beginning and gradually stabilizes at a lower current density. The cathodic current discloses that the samples are cathodically protected because the corrosion potential of these samples are nobler than the anodic operation potential of −0.1 V.

The metal ions in the solution arising from corrosion are very important in gauging the performance of the bipolar plates. Thus, a post corrosion analysis of the test solution for metal ions is performed to determine the extent of metal dissolution during this process. Here, the dissolved metal ions are determined by ICP and the results are summarized in Table 2. The total metal ion concentrations leached from the bare SS316L are 9.19 ppm and 7.79 ppm after the potentiostatic test in the simulated cathode and anode PEMFC environments, respectively. In contrast, the metal ion concentrations leached from the C/CrN multilayer-coated SS316L are greatly reduced due to the higher chemical inertness and better corrosion resistance as indicated by electrochemical test results. C/CrN-1 exhibits Fe selective dissolution in both the cathode and anode environment and the metal ion concentration is higher than those released from the other C/CrN multilayer-coated samples. This is because that the insufficient carbon coating thickness of C/CrN-1 cannot fully prevent SS316L from corrosion. C/CrN-2 also displays Fe selective dissolution in the cathode environment. The metal ion concentration is lower in the anode environment and being 0.288 ppm. With regard to C/CrN-3 and C/CrN-4, the metal ion concentrations are small in the both cathode and anode environments, and that of C/CrN-4 is the lowest, being 0.193 ppm and 0.236 ppm in the cathode and anode environment, respectively. In conjunction with the electrochemical test results, the ICP results agree well with electrochemical results, indicating that the corrosion resistance is closely related to the carbon coating thickness. The coating thickness of C/CrN-3 is the minimum in order to provide sufficient protection against corrosion.

3.6. Surface morphology after potentiostatic tests

The SEM images of the C/CrN multilayer-coated SS316L after potentiostatic tests are depicted in Fig. 7. Fig. 7(a)–(d) shows the surface morphology after potentiostatic tests under simulated cathode conditions. Several pitting corrosion sites (dark areas) can be found on the surface of C/CrN-1 and C/CrN-2 indicative of pitting corrosion during the potentiostatic tests. Most of the pitting corrosion occurs at the boundary of the carbon granules due to the insufficient carbon coating thickness and explains the larger metal ion concentrations released from C/CrN-1 and C/CrN-2. In contrast, C/CrN-3 and C/CrN-4 show no obvious change in the surface morphology, indicating a C/CrN multilayer coating thickness of 800 nm (carbon coating thickness of 400 nm) can prevent the substrate from corrosion in the simulated cathode environment. The surface morphology of the C/CrN multilayer-coated SS316L after potentiostatic tests under simulated anode conditions are shown in Fig. 7(e)–(h). C/CrN-1 undergoes pitting corrosion, which agrees well with the ICP result. The surface morphologies observed from C/CrN-2, C/CrN-3, and C/CrN-4 do not show an appreciable difference with the exception of some adsorbed white corrosion byproducts on the surface. It should be noted that the circular dark area in Fig. 7(g) is not pitting pore but due to corrosion byproducts adhered on the surface. According to the electrochemical tests, ICP, and SEM results, a minimum coating thickness of 800 nm can yield sufficient protection and such a thin coating reduces the mass production cost.

4. Conclusion

C/CrN multilayer coatings are deposited on SS316L samples by CFUBMSIP. The C/CrN multilayer coatings are composed of carbon granules, compact, and dense. Raman spectroscopy indicates that the carbon coatings possess a high percentage of sp^2 bond as well as an amorphous structure. The ICR results disclose superior surface conductivity due to high percentage of sp^2 bond and co-existence of the CrN coating. The values range from 2.6 to 2.9 mΩ-cm^2 at a compaction force of 150 N cm^{-2}. Increasing the thickness of the carbon coatings over the threshold value only improves the ICR marginally. The potentiodynamic, potentiostatic, and ICP results provide evidence that the corrosion resistance is significantly improved by the C/CrN multilayer coatings as a result of the high chemical inertness. Our results also disclose that the corrosion resistance is closely related to the thickness of the carbon coating. A carbon coating that is too thin, such as those on C/CrN-1 and C/CrN-2, is prone to pitting corrosion as confirmed by SEM and more severe release of metal ions during the potentiostatic tests. A C/CrN multilayer coating with a minimum thickness of 800 nm (C/CrN-3) is required to provide adequate functionality and corrosion resistance. Ultimately, with thinner coating and faster deposition process, this technology is suitable for manufacturing of low-cost and high performance coating for metallic bipolar plates.

Acknowledgments

Financial support was provided by National Natural Science Foundation of China under contract number. 51201106 and 50971091, the Ministry of Science and Technology of the People's

Republic of China (grant no. 2009DFB50350), and Hong Kong Research Grants Council (RGC) General Research Funds (GRF) no. CityU 112510.

References

[1] B.L. Yi, Fuel cell-theory technology application, Chemical Industry Press, Beijing, 2003, 160–161.
[2] Y. Wang, K.S. Chen, J. Mishler, S.C. Cho, X.C. Adroher, Applied Energy 88 (2011) 981–1007.
[3] V. Mehta, J.S. Cooper, Journal of Power Sources 114 (2003) 32–53.
[4] A. Hermann, T. Chaudhuri, P. Spagnol, International Journal of Hydrogen Energy 30 (2005) 1297–1302.
[5] A. Kumar, M. Ricketts, S. Hirano, Journal of Power Sources 195 (2010) 1401–1407.
[6] H. Wang, J.A. Turner, Fuel Cells 10 (2010) 510–519.
[7] B.C.H. Steele, A. Heinzel, Nature 414 (2001) 345–352.
[8] H. Tawfik, Y. Hung, D. Mahajan, Journal of Power Sources 163 (2007) 755–767.
[9] K. Feng, Y. Shen, J. Mai, D. Liu, X. Cai, Journal of Power Sources 182 (2008) 145–152.
[10] P.J. Hamilton, B.G. Pollet, Fuel Cells 10 (2010) 489–509.
[11] A. Tarniowy, R. Mania, M. Rekas, Thin Solid Films 311 (1997) 93–100.
[12] M.C.L. de Oliveira, G. Ett, R.A. Antunes, Journal of Power Sources 206 (2012) 3–13.
[13] Y. Wang, D.O. Northwood, International Journal of Hydrogen Energy 32 (2007) 895–902.
[14] Y. Fu, M. Hou, G. Lin, J. Hou, Z. Shao, B. Yi, Journal of Power Sources 176 (2008) 282–286.
[15] Y. Fu, G. Lin, M. Hou, H. Li, L. Hao, Z. Shao, B. Yi, International Journal of Hydrogen Energy 34 (2009) 453–458.
[16] M. Li, S. Luo, C. Zeng, J. Shen, H. Lin, C. Cao, Corrosion Science 46 (2004) 1369–1380.
[17] Y. Wang, D.O. Northwood, Journal of Power Sources 165 (2007) 293–298.
[18] N.D. Nam, J.G. Kim, W.S. Hwang, Thin Solid Films 517 (2009) 4772–4776.
[19] W.S. Jeon, J.G. Kim, Y.J. Kim, J.G. Han, Thin Solid Films 516 (2008) 3669–3672.
[20] B. Elsener, A. Rota, H. Böhni, Materials Science Forum 44 (1989) 29–38.
[21] M. Zhang, B. Wu, G. Lin, Z. Shao, M. Hou, B. Yi, Journal of Power Sources 196 (2011) 3249–3254.
[22] H. Zhang, G. Lin, M. Hou, L. Hu, Z. Han, Y. Fu, Z. Shao, B. Yi, Journal of Power Sources 198 (2012) 176–181.
[23] R. Tian, Journal of Power Sources 196 (2011) 1258–1263.
[24] K. Feng, Y. Shen, H. Sun, D. Liu, Q. An, X. Cai, P.K. Chu, International Journal of Hydrogen Energy 34 (2009) 6771–6777.
[25] K. Feng, X. Cai, H. Sun, Z. Li, P.K. Chu, Diamond & Related Materials 19 (2010) 1354–1361.
[26] W. Jin, K. Feng, Z. Li, X. Cai, L. Yu, D. Zhou, Journal of Power Sources 196 (2011) 10032–10037.
[27] P.K. Chu, L. Li, Materials Chemistry and Physics 96 (2006) 253–277.
[28] A.C. Ferrari, J. Robertson, Physical Review B 61 (2000) 14095–14107.
[29] J. Robertson, Materials Science and Engineering R: Reports 37 (2002) 129–281.
[30] A.K. Iversen, Corrosion Science 48 (2006) 1036–1058.
[31] R. Tian, J. Sun, International Journal of Hydrogen Energy 36 (2011) 6788–6794.